# Timescales of glacial isostatic adjustment in Greenland: is transient rheology required?

Linda Pan [1], Jerry X. Mitrovica,[1] Glenn A. Milne,[2] Mark J. Hoggard [3] and Sarah A. Woodroffe[4]

[1] *Department of Earth and Planetary Sciences, Harvard University, Cambridge, MA 02138, USA . E-mail: lindapan@g.harvard.edu*
[2] *Department of Earth and Environmental Sciences, University of Ottawa, Ottawa, ON K1N 6N5, Canada*
[3] *Research School of Earth Sciences, Australian National University, Canberra, ACT 0200, Australia*
[4] *Department of Geography, Durham University, Durham DH1 3LE, UK*

## SUMMARY

The possibility of a transient rheological response to ice age loading, first discussed in the literature of the 1980s, has received renewed attention. Transient behaviour across centennial to millennial timescales has been invoked to reconcile apparently contradictory inferences of steady-state (Maxwell) viscosity based on two distinct data sets from Greenland: Holocene sea-level curves and Global Navigation Satellite System (GNSS) derived modern crustal uplift data. To revisit this issue, we first compute depth-dependent Fréchet kernels using 1-D Maxwell viscoelastic Earth models and demonstrate that the mantle resolving power of the two Greenland data sets is highly distinct, reflecting the differing spatial scale of the associated surface loading: the sea-level records are sensitive to viscosity structure across the entire upper mantle while uplift rates associated with post-1000 CE fluctuations of the Greenland Ice Sheet have a dominant sensitivity to shallow asthenosphere viscosity. Guided by these results, we present forward models which demonstrate that a moderate low viscosity zone beneath the lithosphere in Maxwell Earth models provides a simple route to simultaneously reconciling both data sets by significantly increasing predictions of present-day uplift rates in Greenland whilst having negligible impact on predictions of Holocene relative sea-level curves from the region. Our analysis does not rule out the possibility of transient deformation, but it suggests that it is not required to simultaneously explain these two data sets. A definitive demonstration of transient behaviour requires that one account for the resolving power of the data sets in modelling the glacial isostatic adjustment process.

**Key words:** Creep and deformation; Loading of the Earth; Sea level change; Transient deformation.

## 1 INTRODUCTION

Studies of glacial isostatic adjustment (GIA) have typically assumed that the deformation of the planet can be modelled with a linear viscoelastic rheology, and generally as a Maxwell material in which the non-elastic response is governed by a steady-state (time-invariant) viscosity (e.g. Peltier 1974). A suite of studies in the 1980s explored the possible role of transient rheology in the GIA process, most often by invoking a Burgers body model and focusing on the lower mantle (Peltier *et al.* 1980, 1986; Peltier 1985; Sabadini *et al.* 1985, 1987; Yuen *et al.* 1986). These papers were motivated by the apparent inconsistency between inferences of the radial profile of mantle viscosity based on GIA records (Cathles 1975; Peltier & Andrews 1976; Wu & Peltier 1983) and contemporaneous studies of the long

wavelength geoid anomalies related to the mantle convection process (Hager 1984; Ricard *et al.* 1984; Richards & Hager 1984; Forte & Peltier 1987), with the latter suggesting a lower-mantle viscosity an order of magnitude greater than the former. However, later work demonstrated that this inconsistency could be reconciled by accounting for the distinct radial resolving power of the two data sets (Mitrovica 1996), and that multilayer models with a significant, two order of magnitude viscosity increase with depth, simultaneously reconciled both data sets (Forte & Mitrovica 1996; Mitrovica & Forte 2004). Consequently, interest in transient rheology within the GIA community declined.

In subsequent years, and leading to the present day, modelling of transient rheology has been a central theme in studies of post-seismic deformation (Pollitz 2003; Freed & Bürgmann 2004;

Hetland & Hager 2006; Han *et al.* 2008; Cannelli *et al.* 2010; Hoechner *et al.* 2011; Muto *et al.* 2019). Moreover, experimental studies have suggested various microphysical processes that may give rise to linear (Faul & Jackson 2015) or nonlinear (Karato 2021) transient behaviour. Motivated, at least in part, by these studies, recent efforts have focused on deriving generalized rheological models that can encompass viscoelastic dissipation over timescales ranging from decadal to centennial (Ivins *et al.* 2020) or, even more broadly, from minutes and hours (seismic normal modes) to millions of years (mantle convection) (Lau & Holtzman 2019).

Because of these studies, interest in transient rheological models within the GIA literature has renewed. Simon *et al.* (2022) compared predictions of sea-level change at widely distributed sites since the Last Glacial Maximum (LGM) using Burgers body models with varying creep parameters to analogous predictions based on Maxwell viscoelastic rheology. They argued that transient behaviour would be most evident in the near field of ice sheets during periods of rapid ice mass flux. Adhikari *et al.* (2021) inferred transient behaviour in Greenland data sets by noting that Maxwell models that fit Holocene sea-level records from the region preferred uniform upper-mantle viscosity values close to $5 \times 10^{20}$ Pa·s, while modern, GNSS-determined uplift rates driven by ice mass changes could only be fit if deformation associated with ice mass flux since 1000 CE was modelled with a uniform upper-mantle viscosity in the range $0.6–1.1 \times 10^{20}$ Pa·s. Paxman *et al.* (2023) explored this apparent contradiction using a spectrum of transient models. They concluded that such models were likely important to modelling of loading and deformation on centennial to millennial timescales in Greenland and could reconcile the uplift rate observations with the Holocene sea-level record.

Following the logic of Mitrovica (1996), it may be possible to fit both the GNSS uplift rates and sea-level records if these two observational data sets have distinct resolving power in their sensitivity to mantle viscosity and if one relaxes the assumption in the modelling of Adhikari *et al.* (2021) of a uniform upper-mantle viscosity. There is reason to believe that the resolving power of the data sets will differ given that reconstructions of post-LGM mass flux in Greenland (Lecavalier *et al.* 2014) have a broader spatial extent than mass flux inferred since 1000 CE, which is largely localized to the perimeter of the ice sheet (Kjeldsen *et al.* 2015). In the results below, we explore this issue by combining a resolving power analysis and forward modelling of the two data sets to quantify the extent to which the observations have independent sensitivities and whether this provides a route to simultaneously reconciling them with a steady-state viscosity model. Our goal is not to rule out the possible presence of transient rheologies but rather to consider whether these Greenland data sets *require* such deformation.

## 2 METHODS

All GIA predictions herein will be performed using 1-D Maxwell viscoelastic Earth models with elastic structure given by the Preliminary Reference Earth Model (PREM; Dziewonski & Anderson 1981), and an elastic lithosphere of thickness 75 km. We will consider two viscosity models discussed by Adhikari *et al.* (2021). The first has a uniform upper-mantle viscosity of $5 \times 10^{20}$ Pa·s, as favoured by Holocene sea-level records (Lecavalier *et al.* 2014; henceforth model $V_H$), and the second ($V_L$) with a uniform upper-mantle viscosity of $10^{20}$ Pa·s, as required by Adhikari *et al.* (2021) to fit uplift rate observations. We also consider a series of additional

models identical to $V_H$, except for the addition of a low viscosity zone below the lithosphere with varying combinations of layer thickness and viscosity. As an example of nomenclature, a model with a low viscosity zone of 45 km thickness and viscosity $10^{19}$ Pa·s is denoted as LVZ45/$10^{19}$. All models have a lower-mantle viscosity of $2 \times 10^{21}$ Pa·s, however the forward predictions are relatively insensitive to this choice (as will be clear from the Fréchet kernels shown below).

We adopt two ice histories discussed in the literature. The first is the Huy3 ice history developed by Lecavalier *et al.* (2014) in their analysis of Holocene sea-level records from Greenland. Fig. 1(a) shows the change in ice thickness in this model from 25 ka to the present day. Outside of Greenland, Lecavalier *et al.* (2014) adopted the nn9927 model reconstruction for the North American ice sheets (Tarasov *et al.* 2012) and the ICE-5 G model of Peltier (2004) for all other ice sheets. The second ice history was derived by Adhikari *et al.* (2021, henceforth A2021) based on the work of Kjeldsen *et al.* (2015). The A2021 model involves an advance of the Greenland Ice Sheet from the end of the Medieval Warm Period from 1000 CE to 1400 CE (the early phase of the Little Ice Age), followed by a period of stability to 1875 CE, and then a retreat back to initial (1000 CE) conditions by the turn of the millennium, 2000 CE (see fig. 2 of Adhikari *et al.* 2021). Fig. 1(b) shows the change in ice thickness from 1875 CE to present for this model, and superimposed on the figure are the location of the 57 GNSS sites adopted in the analysis of Adhikari *et al.* (2021). Note, as suggested in the Introduction, that the zone of melt in the Huy3 model is of broader spatial scale than the melt geometry of model A2021.

For each of the above ice histories, gravitationally self-consistent sea-level changes are computed using a pseudo-spectral theory that incorporates evolving shorelines, changes in the perimeter of grounded marine-based ice sheets, and the feedback of Earth rotation changes into sea level (Kendall *et al.* 2005; Mitrovica *et al.* 2005). The same theory outputs radial uplift rates. We adopt a truncation at spherical harmonic degree and order 1024 for calculations based on A2021 and at 256 for calculations using Huy3. This difference is reflective of the different resolutions of the ice histories.

In addition to forward predictions of sea-level change and crustal uplift rates, we compute Fréchet kernels, $F$, for these predictions using the numerical approach described by Mitrovica & Peltier (1991). Fréchet kernels are functions of radius, $r$, and viscosity profile $\upsilon(r)$, and they relate logarithmic perturbations in the viscosity profile to the perturbation in any given data point prediction, $\delta y_i$, via the following expression:

$$\delta y_i = \int_{CMB}^{LAB} F_i \left( \log \upsilon, r \right) \delta \log \upsilon \left( r \right) dr, \tag{1}$$

where CMB and LAB represent the radius of the core–mantle and lithosphere–asthenosphere boundaries, respectively. The amplitude of the Fréchet kernel at any depth reflects the sensitivity of the data point prediction to perturbations in viscosity at that depth. To compute the kernels, we discretize the sublithospheric mantle into 43 layers of uniform viscosity and perform forward calculations in which a perturbation in viscosity is applied to each layer in turn. In each case, eq. (1) collapses to a form in which the value of $F$ at the layer of perturbed viscosity can be estimated.

## 3 RESULTS AND DISCUSSION

Fréchet kernels for present-day uplift rates at 57 sites in the GNSS database (Fig. 1b) are shown in Figs 2(a) and (b) for calculations based on the post-LGM ice history Huy3 and the post-1000 CE
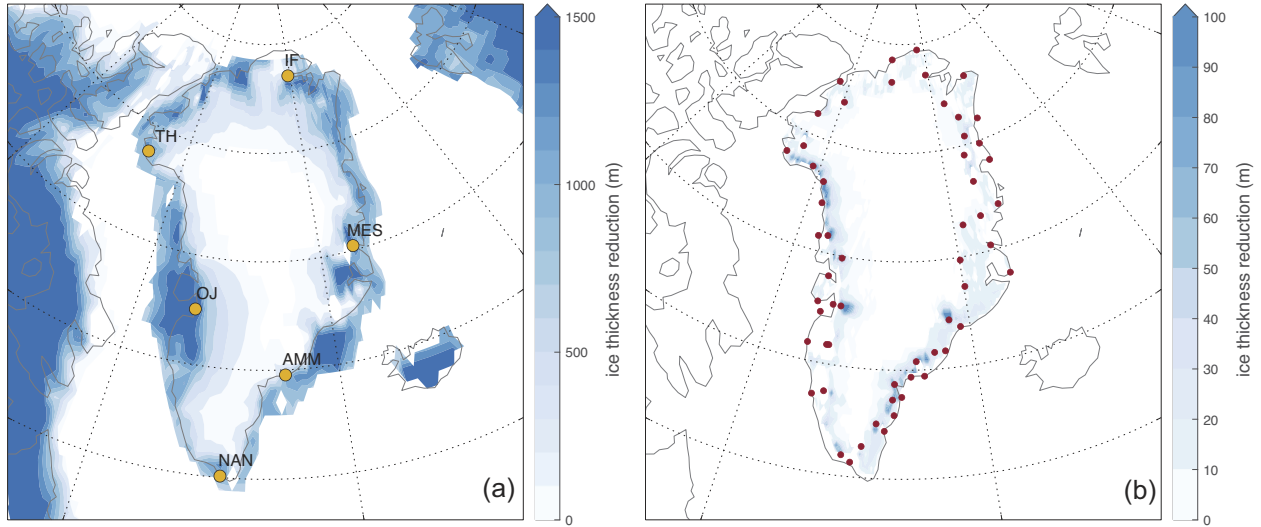
**Figure 1.** Ice history models. Reduction in ice thickness over Greenland in the: (a) Huy3 ice history (Lecavalier *et al.* 2014) from 25 ka to present; and (b) the A2021 ice history (Adhikari *et al.* 2021) from 1875 CE to present. Superimposed in (a) are markers showing the locations of Holocene sea-level records considered in Fig. 5 (MES is Mesters Vig, IF is Independence Fjord, TH is Thule, OJ is Outer Jakobshavn, NAN is Nanortalik and AMM is Ammassalik). The markers in (b) provide the locations of 57 permanent GNSS stations used to determine uplift rates discussed in the text and considered in Fig. 3 (see Supporting Information Fig. S1 for individual site numbers).
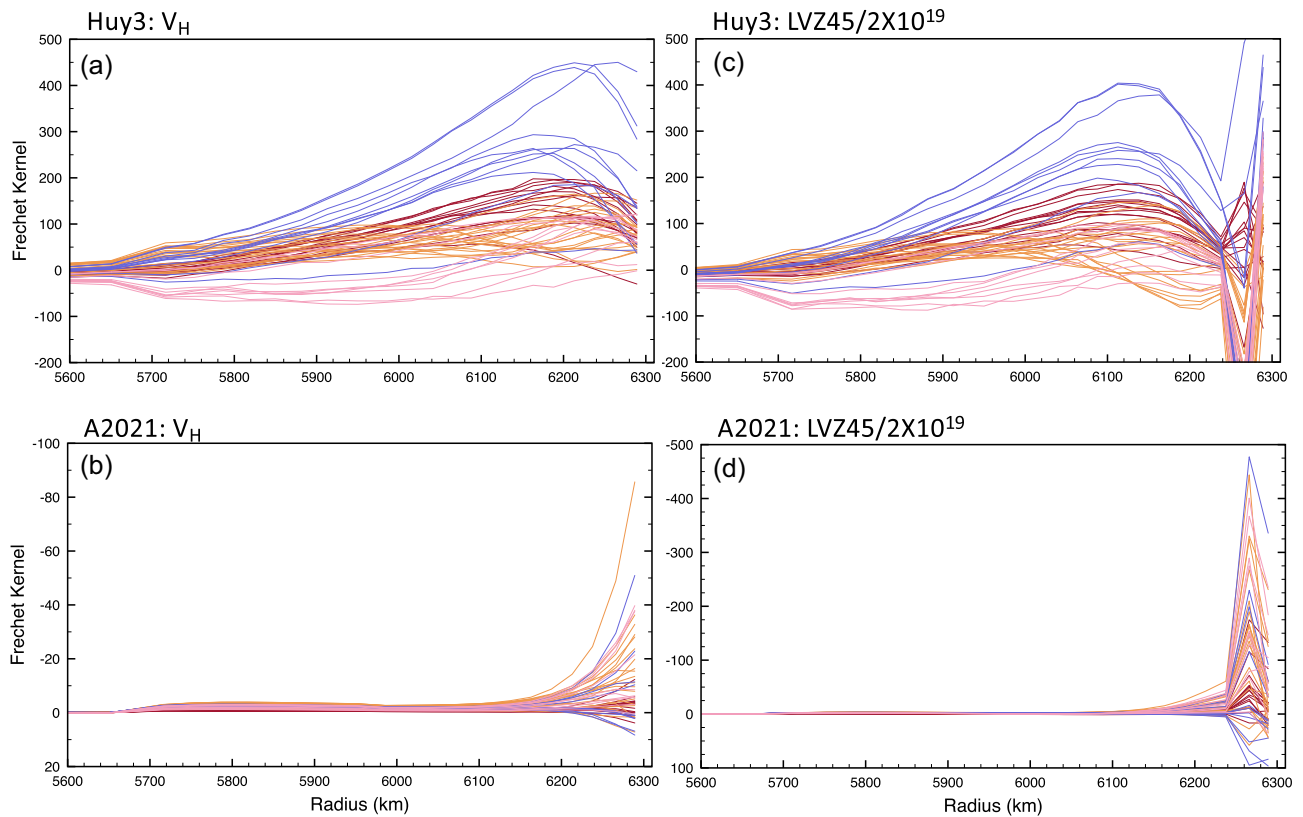


**Figure 2.** Fréchet kernels for Greenland uplift rate predictions. Fréchet kernels defined in the main text (eq. 1) at all 57 GNSS sites (Fig. 1b). While these kernels extend to the CMB, we only plot values within the upper mantle. Frames A and B are computed with the $V_H$ Earth model characterized by an elastic lithospheric thickness of 75 km, and upper and lower-mantle viscosity of $5 \times 10^{20}$ and $2 \times 10^{21}$ Pa·s, respectively. Frames (c) and (d) are analogous to (a) and (b) except that a 45 km zone of viscosity $10^{19}$ Pa·s is introduced in the Earth model below the LAB (model LVZ45/$10^{19}$). Frames (a) and (c) are computed using the Huy3 ice history (Fig. 1a; Lecavalier *et al.* 2014), and frames (b) and (d) are based on the post-1000 CE ice history A2021 (Adhikari *et al.* 2021). These kernels are shaded to coincide with shading of sites in Supporting Information, Fig. S1.
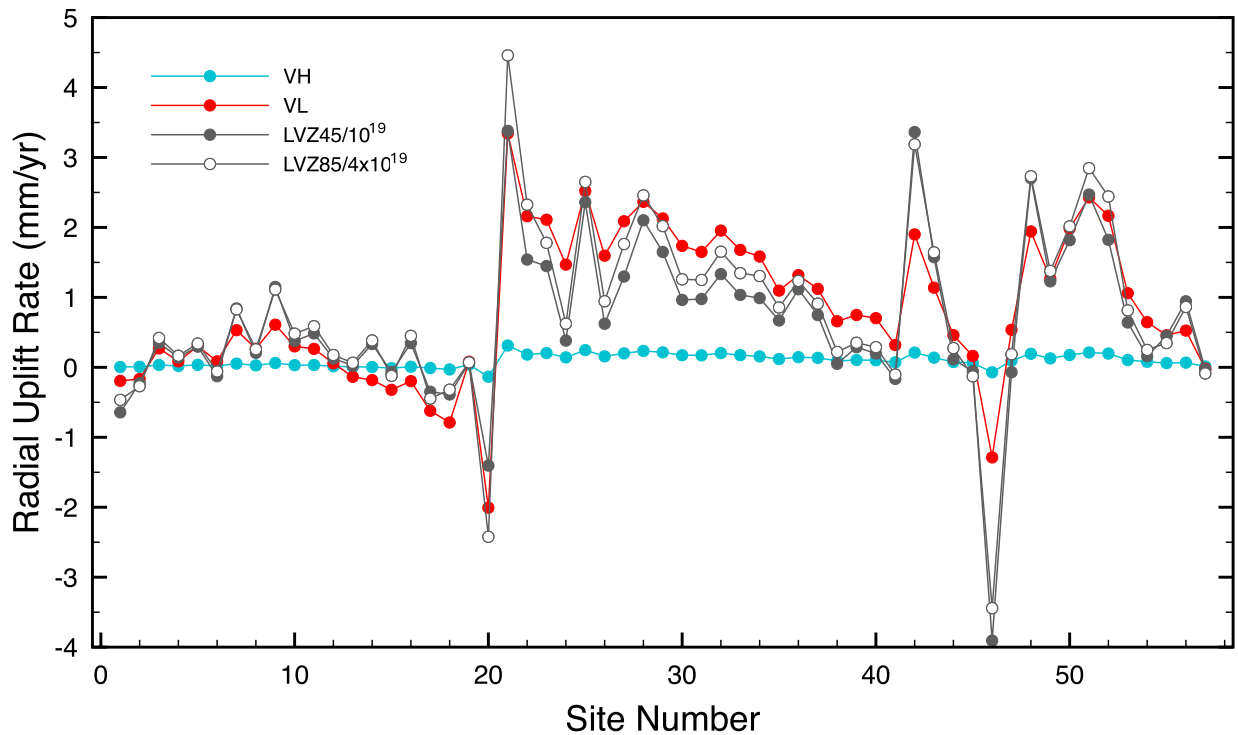
**Figure 3.** Predicted uplift rates. Predictions of present-day crustal uplift rates at all 57 GNSS sites (Fig. S1, Supporting Information) generated with the post-1000 CE ice history A2021 (Adhikari *et al.* 2021). Cyan: predictions generated with the $V_H$ Earth model characterized by an elastic lithospheric thickness of 75 km, and upper- and lower-mantle viscosity of $5 \times 10^{20}$ and $2 \times 10^{21}$ Pa·s, respectively. Red: predictions analogous to the blue, except for the model $V_L$, in which the upper-mantle viscosity is reduced to $10^{20}$ Pa·s. Solid and open grey circles—predictions analogous to the cyan, except that a 45 km zone of viscosity $10^{19}$ Pa·s (model LVZ45/$10^{19}$) or 85 km zone of viscosity $4 \times 10^{19}$ Pa·s is introduced below the LAB (model LVZ85/$4 \times 10^{19}$).
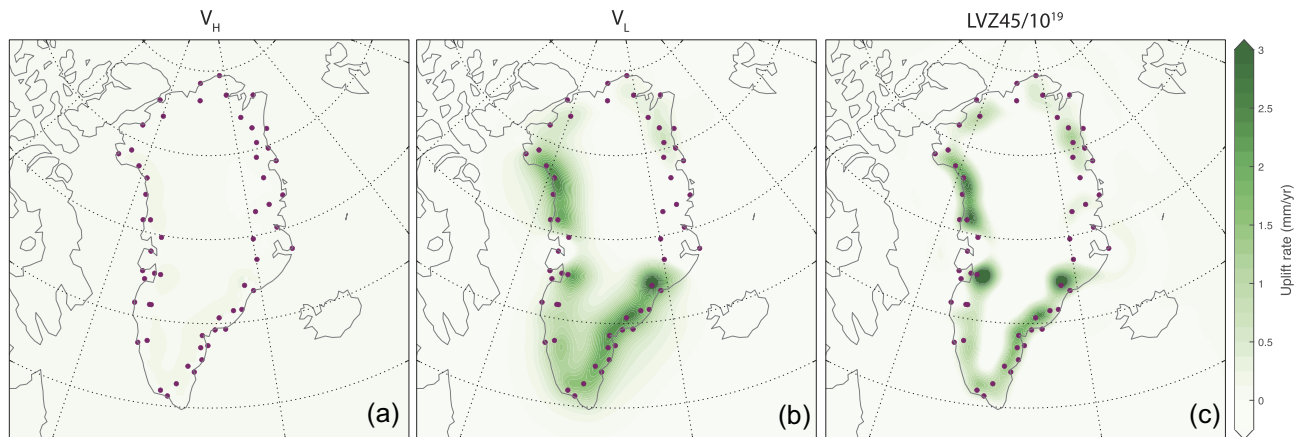


**Figure 4.** Maps of predicted uplift rate. Predictions of present-day crustal uplift rates over Greenland generated with: (a) the $V_H$ Earth model characterized by an elastic lithospheric thickness of 75 km, and upper- and lower-mantle viscosity of $5 \times 10^{20}$ and $2 \times 10^{21}$ Pa·s, respectively; (b) the $V_L$ Earth model, in which the upper-mantle viscosity is reduced to $10^{20}$ Pa·s and (c) the LVZ45/$10^{19}$ model in which a 45 km deep zone of viscosity $10^{19}$ Pa·s is introduced below the LAB and the remaining upper mantle has a viscosity fixed to $5 \times 10^{20}$ Pa·s. All predictions are generated with the post-1000 CE ice history A2021 (Adhikari *et al.* 2021). The markers provide the locations of 57 permanent GNSS stations used to determine uplift rates discussed in the text and considered in Fig. 3.

ice history A2021, respectively. In both cases, we have adopted the Earth model $V_H$, with upper-mantle viscosity $5 \times 10^{20}$ Pa·s. Both sets of kernels tend to peak toward the shallowest part of the upper mantle; however, in contrast with the A2021 kernels, the Huy3 kernels show significant sensitivity to variations in viscosity throughout the entire upper mantle. This difference reflects, as noted above, the broader spatial scale of the Huy3 melt geometry relative to the A2021 geometry (Fig. 1). We have quantified this difference by computing the integrated area under each of the curves in the radial

regions extending from 5700 to 6200 km (i.e. transition zone to base of asthenosphere) and 6200 km to the LAB (i.e. asthenosphere). The ratio between the sum of the magnitudes of the former to the latter for the Huy3 based calculations is 3.0 and for the A2021 based kernels it is 1.4.

As noted in eq.Equation (1), these Fréchet kernels are functions of the underlying viscosity profile, and we have repeated the calculations by introducing a thin, 45 km, zone of viscosity $2 \times 10^{19}$ Pa·s below the lithosphere into an upper mantle of viscosity $5 \times 10^{20}$ Pa·s
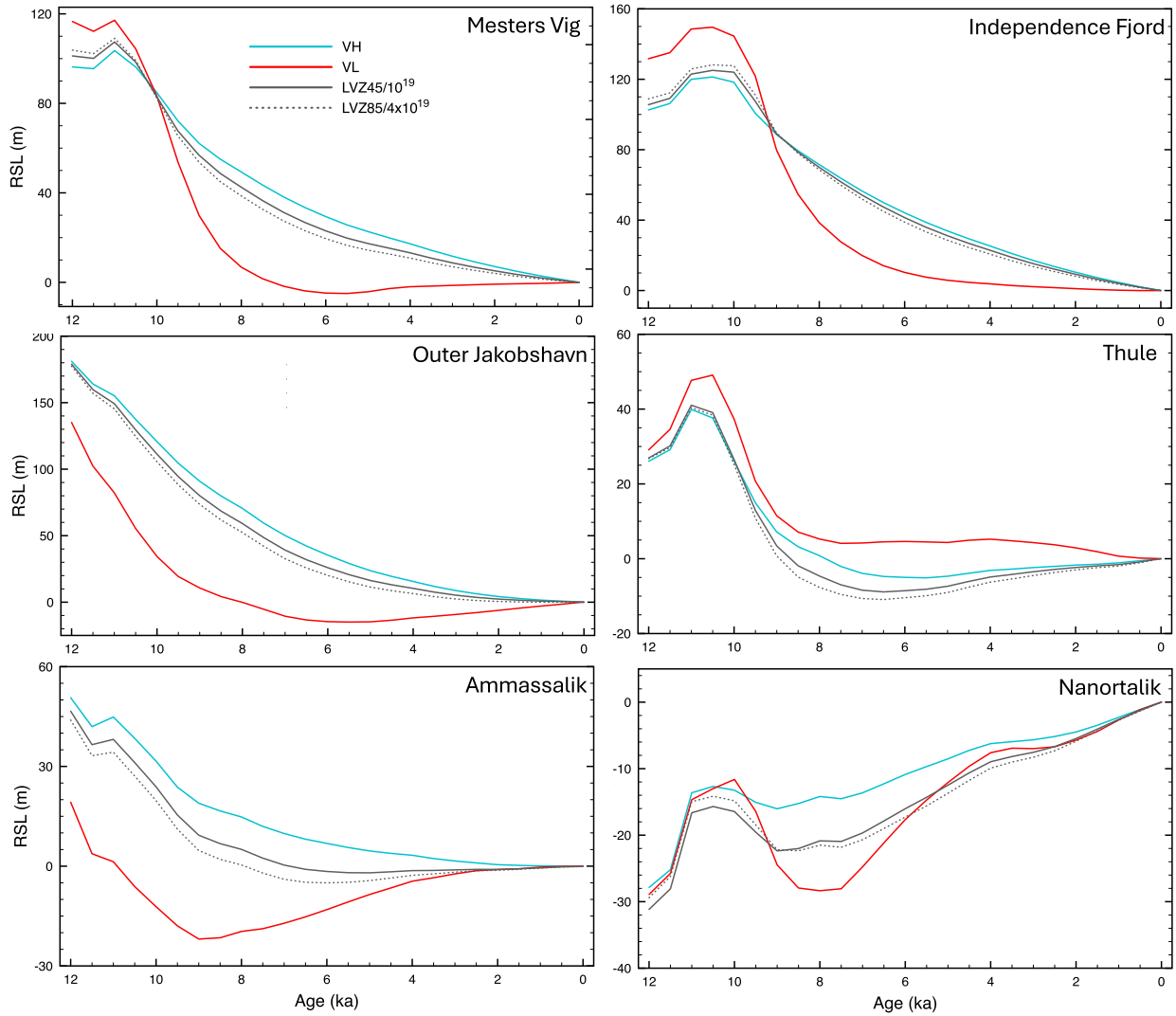
**Figure 5.** Relative sea-level predictions. Prediction of relative sea-level change at six sites in Greenland, as labelled at top right, computed with: cyan line—the $V_H$ Earth model characterized by an elastic lithospheric thickness of 75 km, and upper- and lower-mantle viscosity of $5 \times 10^{20}$ and $2 \times 10^{21}$ Pa·s, respectively; red line—$V_L$ model in which the upper-mantle viscosity is reduced to $10^{20}$ Pa·s; and grey solid and dashed lines—models LVZ45/$10^{19}$ and LVZ85/$4 \times 10^{19}$ in which a 45 km deep zone of viscosity $10^{19}$ Pa·s or 85 km deep zone of viscosity $4 \times 10^{19}$ Pa·s, respectively, are introduced below the LAB and the remaining upper mantle has a viscosity fixed to $5 \times 10^{20}$ Pa·s. All predictions are generated with the Huy3 ice history discussed in the text (Lecavalier *et al.* 2014). Locations of the six sites are shown in Fig. 1(a).

(i.e. model LVZ45/$2 \times 10^{19}$). The results for the Huy3 and A2021 loading history are shown in Figs 2(c) and (d), respectively. The introduction of the low viscosity zone has a minor effect on the Huy3 based calculations, with increased structure in shallower regions, and the above sensitivity ratio becomes 4.1. In contrast, the introduction of the low viscosity zone shifts the sensitivity of the A2021 uplift rate predictions into the shallow asthenosphere, and the above sensitivity ratio becomes 0.2. We conclude that predictions based on the Huy3 ice history are relatively insensitive to the introduction of the low viscosity zone, but that the presence of this zone further localizes the sensitivity of predictions based on the A2021 to the shallowest upper mantle. We note, as is clear in Fig. 2, that the same conclusion would hold if we chose the radius of the boundary between the two integration regions (i.e. 6200 km) to be anywhere within the upper mantle.

We next explore these contrasting sensitivities with a series of forward calculations. Fig. 3 shows predictions of present-day uplift rates at the 57 GNSS sites in Greenland based on the A2021 ice history and the $V_H$, $V_L$, LVZ45/$10^{19}$, and LVZ85/$4 \times 10^{19}$ Earth models. As noted by Adhikari *et al.* (2021), the $V_H$ model combined with the Huy3 ice history was favoured based on fits to Holocene sea-level records; however, when this ice history was augmented by the post-1000 CE A2021 ice history, the predicted present-day crustal uplift rates were too low to fit the 57 GNSS observations. The fit was significantly improved—and transient viscosity was inferred—by pairing the A2021 ice history with an upper-mantle viscosity reduced from $5 \times 10^{20}$ to $10^{20}$ Pa·s, as in our $V_L$ Earth model. Fig. 3 confirms that this reduction leads to an order of magnitude increase in the uplift rates predicted using the A2021 ice history (blue versus red lines). However, a similar trend in uplift rates is also predicted by adopting the models LVZ45/$10^{19}$ and LVZ85/$4 \times 10^{19}$. That is, as suggested by the Fréchet kernels in Figs 2(b) and (d), the introduction of a thin zone of relatively moderate low viscosity has the same impact on the uplift rate predictions based on the A2021 ice history

as decreasing the uniform upper-mantle viscosity from $5\times10^{20}$ Pa·s (model $V_H$) to $10^{20}$ Pa·s ($V_L$). We note from Fig. 3 that there is a trade-off between the thickness and viscosity of the low viscosity zone necessary to increase the uplift rates by a given amount.

Fig. 4 shows a map view of uplift rate predictions based on the A2021 ice history and the $V_H$, $V_L$, and LVZ45/$10^{19}$ Earth models. The thin low viscosity layer of model LVZ45/$10^{19}$ acts to localize the deformation toward the zone of ice mass loss (Fig. 4c) in contrast to the result for model $V_L$, which produces a more diffuse uplift pattern (Fig. 4b). However, the strong similarity between the two fields reinforces the argument that a thin low zone of viscosity $10^{19}$ Pa·s embedded in an upper mantle of viscosity $5\times10^{20}$ Pa·s produces a comparable amplification of uplift rates, relative to predictions based on the $V_H$ model, as a reduction of the upper-mantle viscosity to $10^{20}$ Pa·s. A similar conclusion holds for model LVZ85/$4\times10^{19}$.

The question arises: what impact would a low viscosity zone have on predictions of Holocene sea-level variations based on the Huy3 ice history? The Fréchet kernels in Figs 2(a) and (c), albeit associated with uplift rate predictions, suggest that this impact would be more muted than a reduction in the viscosity of the entire upper mantle. This expectation is confirmed in Fig. 5, where we show predictions of relative sea level since 12 ka at a representative set of six sites in the database considered by Lecavalier *et al.* (2014, as labelled; see Fig. 1a for locations). The predictions adopt the Huy3 ice history of that study, and the same four Earth models considered in Fig. 3, namely $V_H$, $V_L$, LVZ45/$10^{19}$, and LVZ85/$4\times10^{19}$. A comparison of the results based on Earth models $V_H$ and the two models with a low viscosity zone shows that the introduction of such a zone has a small effect on the predictions relative to the observational uncertainties cited in Lecavalier *et al.* (2014). In contrast, reducing a uniform viscosity of the upper mantle from $5\times10^{20}$ to $10^{20}$ Pa·s leads to a major change in the predicted sea-level histories.

The forward calculations in Figs 3–5 indicate that a fit to Holocene relative sea-level histories using the model $V_H$, as in Lecavalier *et al.* (2014), will be preserved with the introduction of a low viscosity zone below the LAB. However, the same localized feature can simultaneously increase predicted present-day uplift rates by an order of magnitude or more, relative to predictions based on the $V_H$ model, similar to the amplification Adhikari *et al.* (2021) obtained by reducing the uniform upper-mantle viscosity of that model from $5\times10^{20}$ to $10^{20}$ Pa·s.

## 4  CONCLUSIONS

The possibility that the Earth's response to surface mass loading is characterized by transient effects has received renewed attention in the literature of Pleistocene GIA (Adhikari *et al.* 2021; Paxman *et al.* 2023). A robust demonstration of such behaviour would be fundamentally important to modelling the adjustment of the solid Earth in response to loading on decadal to multicentury timescales characteristic of various rapid events across the ice age and potential events in the future of a progressively warming world. However, a definitive demonstration of transient behaviour requires that one accounts for the different resolving power of the data sets in modelling the GIA process. We have shown, for example, that introducing a relatively moderate low viscosity zone beneath the LAB in a Maxwell Earth model provides a route to reconciling Holocene sea-level records and modern crustal uplift rates in Greenland, a combined data set that has alternatively formed the basis of arguments for transient deformation. We emphasize that our analysis does not rule out such deformation, and future work should actively continue to explore

the possibility of such behaviour in GIA data sets, but it suggests that it is not required to simultaneously explain the two distinct data sets, Holocene sea-level records and modern uplift rates, from Greenland. Furthermore, attempts to fit these two data sets should not neglect the presence of uncertainties in the space–time history of the nearby Laurentide Ice Sheet (Lecavalier *et al.* 2014).

## DATA AVAILABILITY

All data necessary to reproduce the results in this paper are available on the public archive Zenodo (doi.org/10.5281/zenodo.10783106). The ice histories adopted in this study are taken from published sources.

## SUPPORTING INFORMATION

Supplementary data are available at *GJI* online.

**Figure S1.** Reproduction of Fig. 1(b) with sites identified by numerical labels adopted from Adhikari *et al.* (2021).

Please note: Oxford University Press is not responsible for the content or functionality of any supporting materials supplied by the authors. Any queries (other than missing material) should be directed to the corresponding author for the paper.

## REFERENCES

Adhikari, S., Milne, G.A., Caron, L., Khan, S.A., Kjeldsen, K.K., Nilsson, J., Larour, E. & Ivins, E.R., 2021. Decadal to centennial timescale mantle viscosity inferred from modern crustal uplift rates in Greenland. *Geophys. Res. Lett.,* **48,** e2021GL094040. doi: 10.1029/2021GL094040.

Cannelli, V., Melini, D. & Piersanti, A., 2010. Post-seismic stress relaxation with a linear transient rheology. *Ann. Geophys.,* **53,** 89–99.

Cathles, L.M., 1975. *Viscosity of the Earth's Mantle,* Princeton University Press.

Dziewonski, A.M. & Anderson, D.L., 1981. Preliminary reference Earth model. *Phys. Earth planet. Inter.,* **25,** 297–356.

Faul, U. & Jackson, I., 2015. Transient creep and strain energy dissipation: an experimental perspective. *Annu. Rev. Earth Planet. Sci.,* **43,** 541–569.

Forte, A.M. & Mitrovica, J.X., 1996. New inferences of mantle viscosity from joint inversion of long-wavelength mantle convection and post-glacial rebound data. *Geophys. Res. Lett.,* **23,** 1147–1150.

Forte, A.M. & Peltier, W.R., 1987. Plate tectonics and aspherical earth structure: the importance of poloidal-toroidal coupling. *J. geophys. Res. Solid Earth,* **92,** 3645–3679.

Freed, A.M. & Bürgmann, R., 2004. Evidence of power-law flow in the Mojave desert mantle. *Nature,* **430,** 548–551.

Hager, B.H., 1984. Subducted slabs and the geoid: constraints on mantle rheology and flow. *J. geophys. Res. Solid Earth,* **89,** 6003–6015.

Han, S.-C., Sauber, J., Luthcke, S.B., Ji, C. & Pollitz, F.F., 2008. Implications of postseismic gravity change following the great 2004 Sumatra-Andaman earthquake from the regional harmonic analysis of GRACE intersatellite tracking data. *J. geophys. Res. Solid Earth,* **113,** B11413. doi: 10.1029/2008JB005705.

Hetland, E.A. & Hager, B.H., 2006. The effects of rheological layering on post-seismic deformation. *Geophys. J. Int.,* **166,** 277–292.

Hoechner, A., Sobolev, S.V., Einarsson, I. & Wang, R., 2011. Investigation on afterslip and steady state and transient rheology based on postseismic deformation and geoid change caused by the Sumatra 2004 earthquake. *Geochem. Geophys. Geosyst.,* **12,** Q07010. doi: 10.1029/2010GC003450.

Ivins, E.R., Caron, L., Adhikari, S., Larour, E. & Scheinert, M., 2020. A linear viscoelasticity for decadal to centennial time scale mantle deformation. *Rep. Prog. Phys.,* **83,** 106801. doi: 10.1088/1361-6633/aba346.

Karato, S.i., 2021. A theory of inter-granular transient dislocation creep: implications for the geophysical studies on mantle rheology. *J. geophys. Res. Solid Earth,* **126,** e2021JB022763. doi: 10.1029/2021JB022763.

Kendall, R.A., Mitrovica, J.X. & Milne, G.A., 2005. On post-glacial sea level—II. Numerical formulation and comparative results on spherically symmetric models. *Geophys. J. Int.,* **161,** 679–706.

Kjeldsen, K.K. *et al.*, 2015. Spatial and temporal distribution of mass loss from the Greenland Ice Sheet since AD 1900. *Nature,* **528,** 396–400.

Lau, H.C.P. & Holtzman, B.K., 2019. "Measures of dissipation in viscoelastic Media" extended: toward continuous characterization across very broad geophysical time scales. *Geophys. Res. Lett.,* **46,** 9544–9553.

Lecavalier, B.S. *et al.*, 2014. A model of Greenland ice sheet deglaciation constrained by observations of relative sea level and ice extent. *Quat. Sci. Rev.,* **102,** 54–84.

Mitrovica, J.X., 1996. Haskell [1935]revisited. *J. geophys. Res. Solid Earth,* **101,** 555–569.

Mitrovica, J.X. & Forte, A.M., 2004. A new inference of mantle viscosity based upon joint inversion of convection and glacial isostatic adjustment data. *Earth planet. Sci. Lett.,* **225,** 177–189.

Mitrovica, J.X. & Peltier, W.R., 1991. A complete formalism for the inversion of post-glacial rebound data: resolving power analysis. *Geophys. J. Int.,* **104,** 267–288.

Mitrovica, J.X., Wahr, J., Matsuyama, I. & Paulson, A., 2005. The rotational stability of an ice-age earth. *Geophys. J. Int.,* **161,** 491–506.

Muto, J., Moore, J.D.P., Barbot, S., Iinuma, T., Ohta, Y. & Iwamori, H., 2019. Coupled afterslip and transient mantle flow after the 2011 Tohoku earthquake. *Sci. Adv.,* **5,** eaaw1164. doi: 10.1126/sciadv.aaw1164.

Paxman, G.J.G., Lau, H.C.P., Austermann, J., Holtzman, B.K. & Havlin, C., 2023. Inference of the timescale-dependent apparent viscosity structure in the upper mantle beneath Greenland. *AGU Adv.,* **4,** e2022AV000751. doi: 10.1029/2022AV000751.

Peltier, W.R., 1974. The impulse response of a Maxwell Earth. *Rev. Geophys.,* **12,** 649–669.

Peltier, W.R., 1985. New constraints on transient lower mantle rheology and internal mantle buoyancy from glacial rebound data. *Nature,* **318,** 614–617.

Peltier, W.R., 2004. Global glacial isostasy and the surface of the ice-age earth: the ICE-5 G (VM2) model and GRACE. *Annu. Rev. Earth planet. Sci.,* **32,** 111–149.

Peltier, W.R. & Andrews, J.T., 1976. Glacial-isostatic adjustment-I. The forward problem. *Geophys. J. Int.,* **46,** 605–646.

Peltier, W.R., Drummond, R.A. & Tushingham, A.M., 1986. Post-glacial rebound and transient lower mantle rheology. *Geophys. J. Int.,* **87,** 79–116.

Peltier, W.R., Yuen, D.A. & Wu, P., 1980. Postglacial rebound and transient rheology. *Geophys. Res. Lett.,* **7,** 733–736.

Pollitz, F.F., 2003. Transient rheology of the uppermost mantle beneath the Mojave Desert, California. *Earth planet. Sci. Lett.,* **215,** 89–104.

Ricard, Y., Fleitout, L. & Froidevaux, C., 1984. Geoid heights and lithospheric stresses for a dynamic Earth. *Ann. Geophys.,* **2,** 267–286.

Richards, M.A. & Hager, B.H., 1984. Geoid anomalies in a dynamic Earth. *J. geophys. Res. Solid Earth,* **89,** 5987–6002.

Sabadini, R., Smith, B.K. & Yuen, D.A., 1987. Consequences of experimental transient rheology. *Geophys. Res. Lett.,* **14,** 816–819.

Sabadini, R., Yuen, D.A. & Gasperini, P., 1985. The effects of transient rheology on the interpretation of lower mantle viscosity. *Geophys. Res. Lett.,* **12,** 361–364.

Simon, K.M., Riva, R.E.M. & Broerse, T., 2022. Identifying geographical patterns of transient deformation in the geological sea level record. *J. geophys. Res. Solid Earth,* **127,** e2021JB023693. doi: 10.1029/2021JB023693.

Tarasov, L., Dyke, A.S., Neal, R.M. & Peltier, W.R., 2012. A data-calibrated distribution of deglacial chronologies for the North American ice complex from glaciological modeling. *Earth planet. Sci. Lett.,* **315-316,** 30–40.

Wu, P. & Peltier, W.R., 1983. Glacial isostatic adjustment and the free air gravity anomaly as a constraint on deep mantle viscosity. *Geophys. J. Int.,* **74,** 377–449.

Yuen, D.A., Sabadini, R.C.A., Gasperini, P. & Boschi, E., 1986. On transient rheology and glacial isostasy. *J. geophys. Res. Solid Earth,* **91,** 11420–11438.